JACS
JOURNAL OF THE AMERICAN CHEMICAL SOCIETY

ARTICLE

pubs.acs.org/JACS

Slow Release of NO by Microporous Titanosilicate ETS-4

Moisés L. Pinto,[†,‡] João Rocha,[*,†] José R. B. Gomes,[†] and João Pires[‡]

[†]Department of Chemistry, CICECO, University of Aveiro, 3810-193 Aveiro, Portugal

[‡]Department of Chemistry and Biochemistry, and CQB, Faculty of Sciences, University of Lisbon, Ed. C8, Campo Grande, 1749-016 Lisboa, Portugal

Supporting Information

ABSTRACT: A novel approach to designing nitric oxide (NO) storage and releasing microporous agents based on very stable, zeolite-type silicates possessing framework unsaturated transition-metal centers has been proposed. This idea has been illustrated with ETS-4 [$Na_9Si_{12}Ti_5O_{38}(OH)\cdot xH_2O$], a titanosilicate that displays excellent NO adsorption capacity and a slow releasing kinetics. The performance of these materials has been compared to the performance of titanosilicate ETS-10, [$(Na,K)_2Si_5TiO_{13}\cdot xH_2O$], of benchmark zeolites mordenite and CaA, and of natural and pillared clays. DFT periodic calculations have shown that the presence of water in the pores of ETS-4 promotes the NO adsorption at the unsaturated (pentacoordinated) Ti^{4+} framework ions.

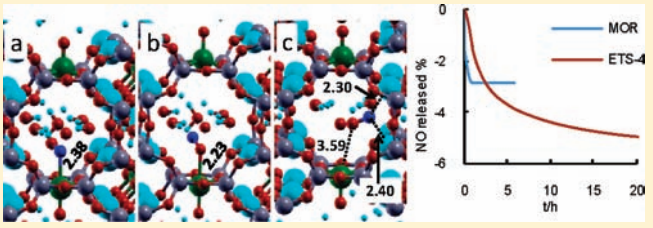

1. INTRODUCTION

In the human body, NO is extremely important in vasodilatation, prevention of platelet aggregation and thrombus formation, neurotransmission, and wound repair.[1] Using exogenous NO in prophylactic and therapeutic processes is a wide-open field. Homogeneous donors that deliver NO directly from solution are established, but they are limited by the systemic nature of delivery, which may cause undesirable side effects. Clearly, new materials and technologies are needed to store and target-deliver NO in biological amounts.[2]

Work on NO storage materials has been concentrated on polymers, whose porosity is not well established.[3] In general, these materials react with NO to form ionic diazeniumdiolates, which release NO in contact with moisture. Zeolites and silicates have a well-known toxicology[4−8] and a deliverable capacity similar to the best diazeniumdiolate polymers. Only a few papers report on the biological activity of NO-releasing zeolites: antithrombosis action on human platelet-rich plasma,[9,10] and no significant inflammation of human skin.[8] Generally, in dehydrated zeolites, NO binds to extra-framework cations and is released after the materials contact with water and cations hydrate. NO may also bind to metal organic frameworks (MOFs) with accessible metal sites in the framework and be used in gas release.[10,11] Certain MOFs have NO adsorption and releasing capacities 5 times greater than zeolites. However, they are less hydrolytically stable than polymers and zeolites, and their toxicology is at its early stage.

Besides good NO adsorption capacity, materials must also present an appropriate releasing kinetics, to maintain a given concentration in the surrounding milieu. Often, a slow releasing kinetics is preferred because it allows for easier and safer control of the NO concentration, for longer periods.

Here, we wish to present a novel approach to designing NO storage and releasing microporous agents based on very stable zeolite-type silicates possessing unsaturated transition-metal centers (e.g., pentacoordinated Ti^{4+}) in the framework, rather than in the pores. We emphasize this is conceptually different from the approaches used so far in the field of conventional zeolites NO storage and release. In a sense, transition metal combines the stability and low toxicity of zeolites with the presence of framework metal centers, as observed in some MOFs. Here, we shall focus on the important family of microporous (stoichiometric) titanosilicates known as ETS (Engelhard titanosilicates) materials, in particular ETS-4 [$Na_9Si_{12}Ti_5O_{38}(OH)\cdot xH_2O$][12] and ETS-10 [$(Na,K)_2Si_5TiO_{13}\cdot xH_2O$].[13] Both solids contain hexacoordinated framework Ti^{4+} ions, although in ETS-4 there is also pentacoordinated Ti^{4+}. We show that the presence of this unsaturated Ti center affords ETS-4 unique NO release properties. Although no biological applications are presented, this work is a first step toward assessing the real potential therapeutic applications of these materials.

2. EXPERIMENTAL SECTION

2.1. Materials. CaA and Mordenite (MOR), supplied by BDH, were manufactured by Linde Air Products. The natural clay, previously characterized,[1] was obtained from soil deposits in Porto Santo (Madeira archipelago). The fraction <63 μm was decarbonated and washed, in a dialysis tube, until a conductivity lower than 1 mS m^{-1} was attained. The pillared clay (PILC) was obtained from the treated natural clay, and the

Received: January 23, 2011
Published: March 30, 2011

dx.doi.org/10.1021/ja200663e | J. Am. Chem. Soc. 2011, 133, 6396–6402

pillaring was preformed with oligomeric cations of aluminum using an optimized procedure.[14,15]

Titanosilicate ETS-10 was synthesized according to the procedure described by Rocha et al.[16] The synthesis of ETS-4 was performed as follows: an alkaline solution was made by dissolving 33.16 g of metasilicate (BDH), 2.00 g of NaOH (Merck), and 3.00 g of KCl (Merck) into 25.40 g of H_2O. 31.88 g of $TiCl_3$ (15% m/m $TiCl_3$ and 10% m/m HCl, Merck) was added to this solution and stirred thoroughly. This gel, with a molar composition $5.9Na_2O{:}0.7K_2O{:}5.0SiO_2{:}1.0TiO_2{:}114H_2O$, was transferred to a Teflon-lined autoclave and treated at 230 °C for 17 h under autogenous pressure without agitation. The product was filtered off, washed at room temperature with distilled water, and dried at 70 °C overnight, the final product being an off-white microcrystalline powder.

2.2. Methods. Nitrogen (Air Liquid, 99.999%) adsorption isotherms were determined in a volumetric automatic apparatus (Micromeritics, ASAP 2010), at −196 °C using a liquid nitrogen cryogenic bath. The samples, between 50 and 100 mg, were outgassed for 3 h at a pressure lower than 0.133 Pa. The degassing temperature was 300 °C for all samples, except ETS-4 for which a temperature of 100 °C was used to prevent pore shrinkage due to dehydration.

The kinetic adsorption profiles of NO in the adsorbent materials were determined in a balance (C. I. Electronics, Disbal) suited for vacuum connected to a high vacuum pump system composed by a turbomolecular pump and a diaphragm pump (Pfeiffer Vacuum). Samples were outgassed in vacuum better than 10^{-2} Pa, during 3 h, using the same temperature as in the nitrogen adsorption experiments. NO was then introduced in the system until a pressure of 80 kPa was attained. The balance was connected to a computer, and the weight was recorded at fixed time intervals between one and two points per minute, during 3 days. Pressure readings were made with a capacitance transducer (Pfeiffer Vacuum, CMR 262). The temperature was controlled at 25 °C using a water bath (Grant, GD120), with 0.05 °C precision. The kinetic desorption profiles were fitted with the stretched exponential model $M_t/M_e = 1 - \exp(-(kt)^{\beta})$, which relates the adsorbed amount at a given time (M_t) with the time (t). The parameters that correspond to the equilibrium uptake (M_e), rate constant (k), and exponent (β) were estimated in the fit. This model is frequently applied for the description of adsorption kinetics of gases and vapors on porous adsorbents.[17]

Thermogravimetry with differential scanning calorimetry (TG-DSC) experiments were performed in an apparatus (Setaram, TG-DSC 111) with 0.001 mg and 0.05 mW of precision, between 30 and 300 °C. Samples of about 40 mg in aluminum crucibles were used, with a heating rate of 2 °C min^{-1}, in nitrogen (Air Liquid, 99.995%) flux of 0.5 cm^3 s^{-1} (Brooks Instruments N.V., tube size R-2-15-AA).

For the investigation of the irreversible adsorbed species by infrared adsorption, samples were introduced in glass cells with PTFE vacuum valves. The cells were connected to a vacuum line, and samples were degassed in vacuum better than 10^{-2} Pa, during 3 h, using the same temperature as in the nitrogen adsorption experiments. After being cooled, NO was introduced in the cells, and the pressure was allowed to stabilize at 80 kPa for about 1 h. The valve was closed, and the cell was removed from the vacuum line. Following 1 week with NO inside, the cell was connected again to the vacuum line, and high vacuum was applied during 4 h. The sample was then removed from the cell and immediately analyzed. The diffuse reflectance infrared Fourier transform (DRIFT) spectra were collected on a Nicolet 6700 FTIR spectrometer at 4 cm^{-1} resolution using the Smart Diffuse Reflectance accessory, at room temperature with a DTGS TEC detector. Each collected spectrum was an average of 512 scans of the sample subtracted by the average of 128 background scans.

For the released gas analysis, samples of the materials were introduced in a laboratory made u-shaped glass cell, and treated as described above (investigation of the irreversible adsorbed species). After 1 week in NO atmosphere, vacuum was made in the cell during a short period to remove the gas contained in the cell dead space. The other end of the sample cell was connected to an infrared gas cell, with 10 cm width and NaCl windows, and helium (Praxair, 99.999%) was passed through the system at 10 cm^3 min^{-1} during 5 min. Special care was taken during this operation to avoid air to enter the sample cell. After this, the infrared gas cell was closed, and the spectra were recorded in a Nicolet 6700 FTIR spectrometer at 4 cm^{-1} resolution, with a DTGS TEC detector. Each collected spectrum was an average of 256 scans of the sample subtracted by the average of 128 background scans.

In the oxyhemoblobin assays, about 7 mg of ETS-4 was used. Small glass crucibles with sample were introduced in glass cells with PTFE vacuum valves. The cells were connected to a vacuum line, and samples were degassed in vacuum better than 10^{-2} Pa, during 3 h, at 100 °C. After being cooled, NO was introduced in the cells, and the pressure was allowed to stabilize at 80 kPa for about 1 h. The valve was closed, and the sample was left in contact with NO for 3 days. The cell was then evacuated for 1 min and filled with helium up to atmospheric pressure. The cell was closed and removed from the vacuum line. To start the NO release to the oxyhemoglobin solution, the cell was opened, the crucible removed, and the powder quantitatively added to 3 mL of oxyhemoglobin solution (1 μM) in a quartz container, which was vigorously shaken and the measuring started. These operations were carried as quickly as possible. The experiments were performed in a 0.1 M phosphate buffer, pH 7.4, and the spectrum of the solutions was collected in a UV/vis spectrophotometer (Jasco V-560). Experiments were also conducted with ETS-4 without being loaded with NO. In this case, all of the procedures were the same except for the loading with NO gas. After degassing, the sample cell was filled with helium, and the experiment was carried out in a similar way.

Two different approximations were used to model ETS-4: 3D periodically repeated unit cell and cluster model approaches. The former is the ideal choice to represent the infinite structure of the material, but, due to the large size of the unit cell (380−390 atoms), several restrictions were needed to perform the calculations (number of optimized atoms and k-points were necessarily reduced).

The periodic calculations were performed with the VASP code[18−20] and the PBE exchange-correlation functional proposed by Perdew−Burke−Ernzerhof.[21] The projected augmented-wave (PAW) method due to Blöch[22] and further implemented by Kresse and Joubert[23] was used to describe the effect of core electrons on the valence shells together with a plane-wave basis set to span the valence electronic states. The cutoff energy for the plane-waves and the Monkhorst−Pack k-points grid used were 450 eV and 1 × 1 × 1, respectively. The spin-polarization was considered only in single-point calculations. The positions of the ions were relaxed using the conjugate-gradient algorithm. The criteria for convergence were 10^{-5} eV, in the total energy, and 5×10^{-2} eV/Å, in the forces acting on the ions. A 1 × 2 × 1 unit cell was built from the experimental structure[12] after elimination of the disorder caused by the arrangement of the bridging five-coordinated Ti atoms and cleaning of superimposed oxygen atoms (water molecules) in the crystallographic cell (Figure 1). Hydrogen atoms were added to the latter and their positions were fully relaxed, while the rest of ions were kept at their crystallographic positions. The crystallographic cell vectors were also kept frozen in all calculations. The resulting system (388 atoms in the unit cell) was used in the subsequent calculations where a NO molecule was inserted into the cavity near the Ti^{4+} ion (N- or O-down configurations). In the calculations with the NO fragment, the atomic positions of the TiO_5 (4 equatorial and 1 axial O atoms) moiety and also of the NO molecule were fully relaxed, while all of the other atoms were frozen. From the resulting structures, two sets of calculations were made: (i) spin-polarized single point calculations were performed to compute the interaction energies, and (ii) three water molecules closest to the NO adsorbate were eliminated, and the optimization procedure was resumed.

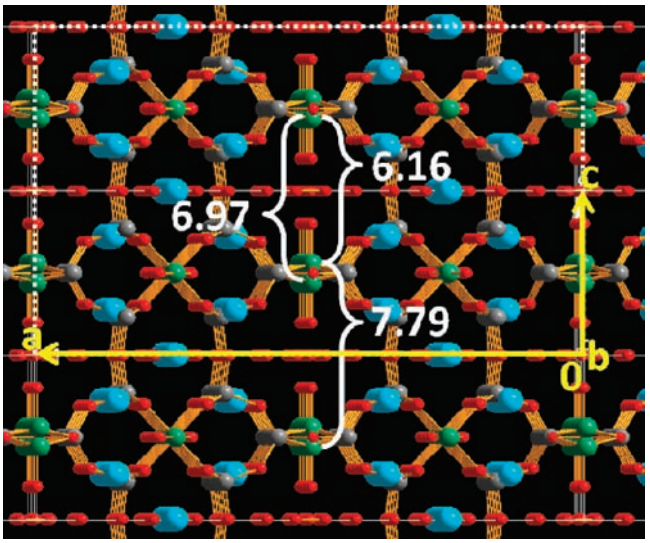

Figure 1. View along vector *b* of the single-crystal X-ray diffraction structure of NaETS-4 showing the disordered pentacoordinated bridging Ti atoms (distances between Ti atoms are in angstroms). The cell vectors and the 1 × 2 × 1 unit cell used in the periodic calculations are shown in yellow and white-dotted lines, respectively. Colored spheres represent atoms of sodium (cyan), oxygen (red), silicon (gray), and titanium (green).

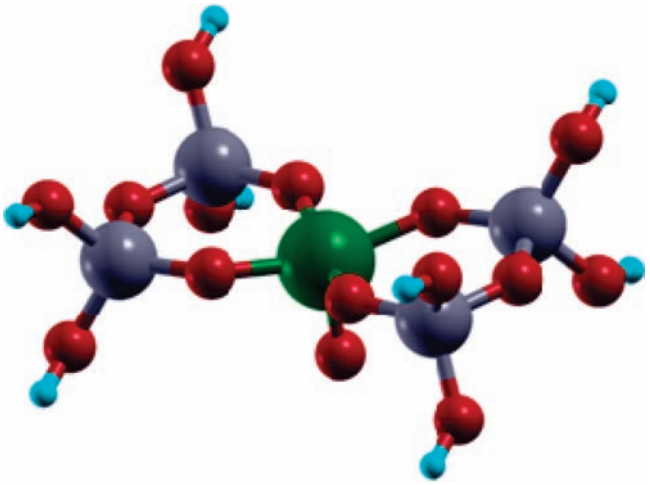

Figure 2. View of the $(TiO_5)Si_4O_{10}H_8$ cluster model. Colored spheres represent atoms of hydrogen (cyan), oxygen (red), silicon (gray), and titanium (green).

The cluster model was also built from the experimental crystallographic structure,[12] but herewith only a few atoms were considered, that is, the $(TiO_5)Si_4O_{10}$ moiety. As usual, hydrogen atoms were introduced for eliminating of dangling bonds into the cluster; the O−H bonds follow exactly the same directions of the O−Si bonds in the experimental crystallographic structure and were fixed to the O atoms at 0.96 Å (mean distance obtained in a previous B3LYP study of several silicates[24]), and the $(TiO_5)Si_4O_{10}H_8$ aggregate was obtained (Figure 2). The positions of the outer $Si_4O_{10}H_8$ moiety were kept frozen in all the calculations. The vertical positions of the Ti and axial O were relaxed, while the *x* and *y* contributions were frozen to keep these atoms at the center of the $Si_4O_{10}H_8$ moiety. The rest of the atoms were fully relaxed except where noticed. The calculations considering the cluster

Table 1. Textural Parameters of the Adsorbent Materials, Calculated from Nitrogen Adsorption Isotherms at −196 °C

	A_{BET}[a] [$m^2\ g^{-1}$]	V_μ[b] [$cm^3\ g^{-1}$]	A_{ext}[b] [$m^2\ g^{-1}$]	V_{tot}[c] [$cm^3\ g^{-1}$]
MOR	507	0.211	20	0.241
CaA	592	0.255	13	0.273
ETS-4	45	0.018	2	0.018
ETS-10	356	0.146	21	0.195
natural clay	95	0.019	52	0.102
PILC	320	0.109	68	0.195

[a] Equivalent surface area (A_{BET}) calculated by the BET equation. [b] Microporous volume (V_μ) and external surface area (A_{ext}) calculated by the *t*-plot method. [c] Total porous (V_{tot}) calculated from the adsorbed amount at $p/p^\circ = 0.95$.[46]

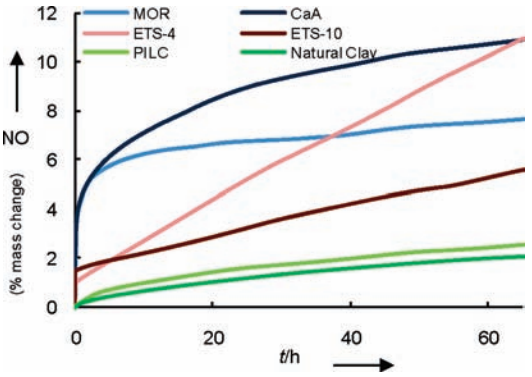

Figure 3. Kinetic profiles of NO adsorption on the studied adsorbent materials, at 80 kPa and 25 °C.

model approach were also performed at the DFT level by means of the B3LYP hybrid functional[25−27] and the Gaussian 03 computer code.[28] The atomic electron densities of the (TiO_5) central unit and of the N and O atoms of the adsorbates were described by the 6-311+G(d,p) basis set,[29,30] while those of the $Si_4O_{10}H_8$ portion considered the LANL2DZ basis set.[31] Finally, the B3LYP frequencies were scaled by a factor of 0.96.[32] This DFT approach was selected because in a very recent study[33] some of us found that this hybrid approach was one of the best exchange-correlation functionals (among 19 that were tested) for the calculation of vibrational frequency shifts for NO adsorbed on nickel-doped MgO(100), a magnetic oxide containing a transition metal known to be hard to model by density functional approximations.

3. RESULTS AND DISCUSSION

The NO adsorption and release properties of microporous titanosilicates ETS-4 and ETS-10 were compared to those of benchmark zeolites mordenite (MOR) and CaA, and natural and pillared (PILC) clays. The adsorbents were characterized by nitrogen adsorption at −196 °C (Figure S1 in the Supporting Information), and the textural parameters obtained from the isotherms are collected in Table 1. NO adsorption was performed on a gravimetric apparatus where samples were outgassed in a vacuum before experiments. Adsorbed amounts (in weight %) are expressed per mass of outgassed material and are thus the NO content of the sample at a given time. The weight change of samples recorded during 3 days afforded the kinetic adsorption curves, at constant pressure (80 kPa) and temperature (25 °C), depicted in Figure 3. Subsequently, the system was evacuated, high vacuum was applied to the samples loaded with NO, and the

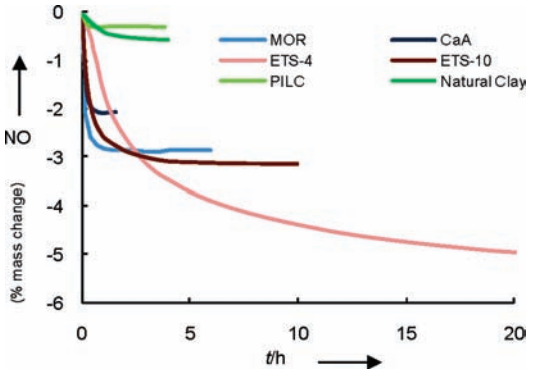

Figure 4. Kinetic profiles of NO desorption on the studied adsorbent materials, in high vacuum at 25 °C, after adsorption at 80 kPa.

weight variation was recorded. This yielded the kinetic desorption curves and an estimate of the NO amount released from the different materials (Figure 4).

The materials have very different NO adsorption capacity (Figure 3) and adsorption kinetics. For instance, after 60 h CaA, ETS-4 adsorbed ca. 11%, mordenite ca. 7.5%, ETS-10 ca. 5.5%, and PILC and natural clays ca. 2% NO. The adsorption capacity is, however, not related to the adsorption kinetics, even for materials with similar adsorption capacity at 60 h. CaA and ETS-4 illustrate this point well: while the amount of NO adsorbed after 60 h is very similar for both materials, after only 20 h does CaA adsorb more NO than ETS-4, by a factor of 2. Careful inspection of Figure 3 and Table 1 reveals that the adsorbed NO amounts are not correlated with the surface areas or pore volumes. A comparison of the NO adsorption kinetics and N_2 adsorption isotherms (Figure S1 in the Supporting Information) supports this conclusion. ETS-4 exhibits both the lowest adsorbed amounts in the nitrogen adsorption isotherms and, in contrast, the highest NO adsorption capacity. In fact, the adsorption capacity observed for ETS-4 (ca. 11% corresponding to 3.7 mmol g^{-1}) is between the 7 and 3 mmol g^{-1} values obtained in MOFs.[10,11]

The shapes of the kinetic adsorption curves bear some similarity in each family of materials (Figure 3). For zeolites (MOR and CaA), the main adsorption occurs up to 10 h, after which the systems approach equilibrium. The clays (PILC and natural clay) exhibit slow rising curves, similar in shape and NO adsorbed amounts. Titanosilicates (ETS-4 and ETS-10) have an initial sharp and small rise in less than 1 h, ascribed to the adsorption on the external surface and pore mouths. Subsequently, a slow process dominates, giving an almost linear variation with time.

After 3 days in NO atmosphere, the materials present clearly different desorption profiles, under high vacuum (Figure 4). Because all samples release (desorb) much less NO than they adsorb, the adsorption process is, to a certain extent, irreversible. Comparison of Figures 3 and 4 also reveals that, for a given material, the NO adsorption and desorption kinetics are different. The slower NO release is observed for ETS-4, for which almost one-half of the previously adsorbed NO is released. This material also shows the slowest adsorption kinetics This relation is, however, not valid for all other materials. For example, PILC presents a slower NO adsorption, but faster desorption, than MOR. The almost linear (i.e., constant) NO release profile in the first hour obtained with ETS-4 is highly desirable for possible therapeutic applications, because it could allow for good control of the NO released to a given system (as a function of time) by varying the loaded ETS-4 dose.

Table 2. Kinetic Desorption Parameters for NO in the Materials, Estimated Using the Stretched Exponential Model

	M_e [%]	k [h^{-1}]	β
MOR	−2.86	5.42	1.26
CaA	−2.05	5.80	1.61
ETS-4	−5.08	0.28	0.72
ETS-10	−3.15	2.22	0.61
natural clay	−0.56	1.15	1.11
PILC	−0.29	15.31	3.01

To better compare the desorption results, a kinetic model was fitted to the data using the nonlinear-least-squares method (see the Supporting Information), and the results are collected in Table 2. The rate constants of the various materials, k, range from 15.31 to 0.28 h^{-1}; although the rate constants of the two zeolites are similar, mordenite releases more NO (smaller M_e). The most interesting material is ETS-4, because it presents the largest NO releasing capacity (ca. 5%, corresponding to 1.7 mmol g^{-1}) and the slowest rate (0.28 h^{-1}). These desorption results are important in the context of a potential NO release application because they allow one to estimate the amount and rate of release. The high-vacuum conditions used correspond to the maximum NO release rate that may be obtained, at ambient temperature, for the studied materials. ETS-4 presents the type of slow release that is required for NO therapeutic applications. ETS-10 is also a suitable material, when faster release rates are required.

The reasons for the different adsorption and desorption behavior of these materials are 2-fold. First, structural disorder actually increases the porosity of ETS-10, while faulting ensures that access to the crystal interior of ETS-4 occurs through the relatively narrow eight-membered rings. Second, NO may coordinate to the unsaturated (pentacoordinated) Ti^{4+} framework ions of ETS-4; this is not possible for ETS-10, which only contains hexacoordinated Ti^{4+}.

Before the adsorption experiment, ETS-4 was outgassed at 100 °C to prevent pore shrinkage at higher temperature, and this relatively low temperature does not fully remove the zeolitic water. Outgassing at 300 °C results in almost no adsorption (<0.7% NO). For ETS-10, the NO adsorption is enhanced when the outgassing temperature is only 100 °C (Figure S2 in the Supporting Information). Because pore shrinkage is not an issue for this material, it may be concluded that the presence of water molecules favors the adsorption of NO on ETS-4 and ETS-10. This aspect was explored further with computational modeling and is discussed later. Interestingly, the NO release profiles are similar for both outgassing temperatures (Figure S2).

To study the amount of NO irreversibly adsorbed on the materials, after desorption under vacuum, the samples were quickly introduced in the TG-DSC apparatus (see Figure S3 in the Supporting Information). For zeolites (CaA and MOR), the weight loss above 300 °C corresponds to the mass of NO not released under vacuum. This means that NO is strongly attached to the surface of these materials, and probably the formation of other nitrogen oxide species takes place.[34−38] In addition, the heat and mass curve profiles of the two zeolites are similar. For ETS-4 and ETS-10, the temperatures for complete NO release are ca. 200 and 150 °C, respectively. For clay materials, small weight losses are observed, which is consistent with the small NO adsorption observed.

Diffuse reflectance infrared Fourier transform spectroscopy (DRIFT) provides further insight into NO adsorption and release

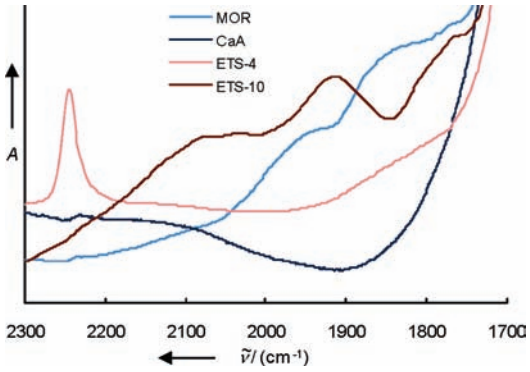

Figure 5. Diffuse reflectance infrared Fourier transform spectra of solids exposed to NO atmosphere during 1 week.

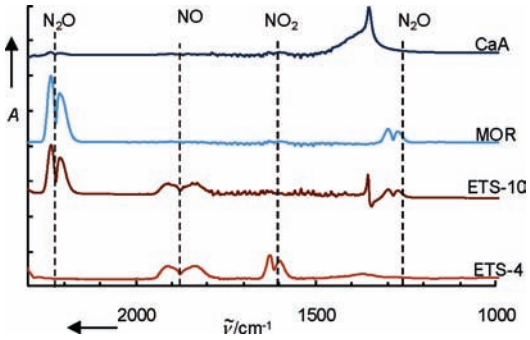

Figure 6. Infrared spectra of the released gas from samples exposed to NO atmosphere during 1 week.

on the most interesting samples. After degassing, samples were closed in glass cells with 80 kPa NO, for 1 week. Vacuum was then applied to the glass cells, and DRIFT spectra were recorded (Figure S4 in the Supporting Information). The 2300−1700 cm^{-1} spectral region is shown in Figure 5. ETS-4 displays a unique and sharp band at 2250 cm^{-1} attributed to adsorbed N_2O,[34,35,37] not observed for the other materials. Density functional theory (DFT) calculations performed on the interaction of NO, NO_2, N_2O, and N_2O_2 species, using a $(TiO_5)Si_4O_{10}H_8$ cluster model, confirm this assignment (see below). Bands at low wave numbers are very broad or appear as shoulders on the water absorption band at 1650 cm^{-1} (not shown, Figure S4). Nevertheless, the ETS-10 and MOR bands at ca. 1930 and 1770 cm^{-1} may be attributed to adsorbed NO^+ and N_2O_2, respectively.[36−39] For ETS-10, a band at ca. 2080 cm^{-1} may be attributed to NO_2^+.[36] ETS-4 and MOR give a shoulder at ca. 1850 cm^{-1}, which may be assigned to adsorbed NO^-.[35,36]

The gas released by CaA, MOR, ETS-4, and ETS-10 was studied by Fourier transform infrared spectroscopy (FTIR). The spectra (Figure 6) show important differences between materials. In particular, NO bands (ca. 1920−1840 cm^{-1}) are present in the spectrum of the gas released from ETS-4 and ETS-10 and are not observed for CaA and MOR. Thus, the gas released from ETS-4 and ETS-10 contains a significant amount of NO. In contrast, CaA and MOR do not seem to be effective in releasing NO, although they present adsorption capacity in kinetic adsorption experiments. The remaining part of the spectra is also informative. Bands at ca. 2260−2200 and 1320−1270 cm^{-1} are attributed do N_2O and are clearly seen for MOR and ETS-10 and fainter in the case of CaA (between 2260−2200 cm^{-1}). The

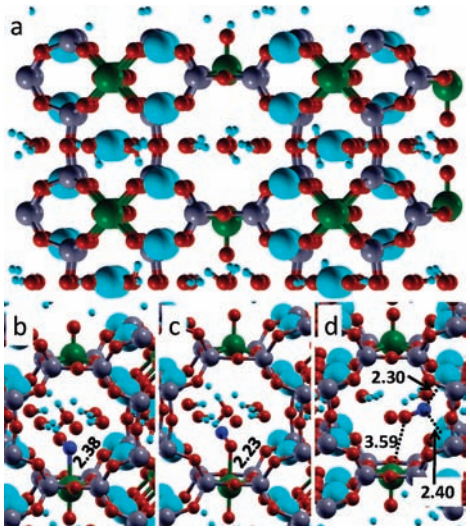

Figure 7. Views of the periodic model (1 × 2 × 1 unit cell built from the experimental cell shown in Figure S5 with disordered Ti atoms and axial oxygen atoms in positions yielding the largest cavity) used in the VASP calculations: (a) full cell; (b) optimized NO (N-down) interacting with the five-coordinate Ti atom; (c) optimized NO configuration with less water molecules in the cavity; and (d) optimized NO (O-down) interacting with the five-coordinate Ti atom. Interatomic distances are in angstroms. Colored spheres represent atoms of sodium (cyan large), hydrogen (cyan small), oxygen (red), nitrogen (blue), silicon (gray), and titanium (green).

NO_2 bands at ca. 1620−1600 cm^{-1} are clearly present in the FTIR spectrum of ETS-4, but they are very faint for MOR and CaA and absent for ETS-10. Considering the areas of the FTIR bands, for ETS-10 the NO/N_2O area ratio is 0.6, while for ETS-4 the NO/NO_2 area ratio is 1.7. This indicates that the NO released from ETS-4 is less contaminated with other gases than the NO released from ETS-10.

To assess the importance of pentacoordinated titanium and the role of water molecules on the adsorption of NO on ETS-4, additional DFT periodic calculations were performed for NO inserted into a large pore of a 1 × 2 × 1 model of the sodium form of ETS-10, NaETS; that is, NO species were introduced into a cavity where the distance between Ti^{4+} framework ions is 7.79 Å and where axial oxygen atoms are pointing outward from the center of the pore (Figures 1 and 7). It was found that the NO molecule interacts with five coordinate Ti^{4+} framework ions (N- or O-down configurations, Figure 7b and c, with interaction energies of 0.33 and 0.47 eV, respectively) if certain water molecules are present in the center of the interstices. Importantly, the elimination of the three water molecules closest to the unsaturated Ti^{4+} ion leads to a configuration where NO interacts with the Na^+ cations (Figure 7d). These findings support the experimental observation that the presence of water promotes the NO adsorption at the unsaturated Ti^{4+} framework ions. Contrary to what happens with NO adsorbed in other zeolites, where the water only mainly promotes the release of NO,[9] the mechanism in ETS-4 is different. In this case, as explained above, water also has a positive effect in the adsorption, increasing the absorbed amounts.

As it can be seen in Table 3, the IR band assignments proposed above for the N_xO_y species are in good accord with the scaled B3LYP frequencies calculated for the gaseous N_xO_y and for the

dx.doi.org/10.1021/ja200663e |J. Am. Chem. Soc. 2011, 133, 6396–6402

Table 3. B3LYP/Cluster Optimized Geometries (Å), Interaction Energies (eV), and Frequencies (cm^{-1})

							frequencies	
species	type	Figure	X−Ti	N−O	N−N	energy[a]	adsorbed	free
NO	N-down top[b]	S5a	2.36 (N)	1.09		−2.02	2094	1899 *1920−1840*[g]
	N-down hollow	S5b	2.67 (N)	1.09		−2.29	2078	
	N-down bridge	S5c	3.12 (N)	1.10		−2.97	1995	
	O-down top[b]	S5d	2.67 (O)	1.10		−1.68	1964 *1930*[c]	
	O-down bridge	S5e	3.28 (O)	1.08		−1.98	2137	
N_2O	N-down top	S5f	2.61 (N)	1.18	1.12	−0.23	2285; 1304 *2250*[d] *2262*;[e] *1313*[e]	2247; 1272 *2260−2200*;[g] *1320−1270*[g]
	O-down top	S5g	2.56 (O)	1.19	1.12	−0.26	2270; 1255 *2250*[d] *2237*;[f] *1251*[f]	
NO_2	η^2-NO	S5h	2.96 (N)	1.14		−1.36	2145; 1273 *2080*[c]	1632; 1334 *1620−1600*[g]
			2.86 (O)	1.14				
N_2O_2	η^2-NN	S5i	2.86 (N)	1.10	2.73	−3.38	2045; 2021	1871; 1704
			2.86 (N)	1.10				
	bridge; not stable[h]	S5j	3.19 (N)	1.11	5.57	−4.51	1986; 1972 *1770*[d]	
			3.19 (N)	1.11				

[a] Energy = $E_{NxOy(TiO5)Si4O10H8} - (E_{NxOy} + E_{(TiO5)Si4O10H8})$. [b] In the case of the bonding atom, only the vertical coordinate was optimized. [c] DRIFT result for a positively charged species, this work. [d] DRIFT result, this work. [e] ONN-Ti (TiO_2 powder); experimental value, ref 47. [f] NNO-Ti (TiO_2 powder); experimental value, ref 47. [g] FTIR result, this work. [h] Not stable as N_2O_2 (N−N bond is cleaved in this cluster model yielding two NO species).

N_xO_y species interacting with the $(TiO_5)Si_4O_{10}H_8$ cluster (Figure 2) except in the case of N_2O_2 where the two B3LYP optimized structures have too elongated or completely cleaved N−N bonds (Figure S5). Importantly, the calculations show that the 2250 cm^{-1} band is compatible with an adsorbed N_2O species (calculated values for N-down and O-down adsorption are 2285 and 2270 cm^{-1}, respectively). The values calculated for the other N_xO_y species interacting with the Ti^{4+} ion are smaller than 2145 cm^{-1} and, thus, differ significantly from the DRIFT value.

The ability of ETS-4 to release biologically relevant NO amounts was tested using the oxyhemoglobin method.[40] The method is based on the principal reaction of oxyhemoglobin with NO to form methemoglobin and nitrate. This reaction also accounts for the inhibitory effect of hemoglobin on the biological effects of endogenous formed or exogenous applied NO. After being loaded with NO, the ETS-4 samples were transferred to a oxyhemoglobin solution, and the changes in the UV/vis spectrum of the solution were recorded. In Figure 8, the changes in the spectrum after 1 h are evident and represent the transformation of oxyhemoblobin to methemoglobin. Comparing the initial spectrum of the oxyhemoglobin solution with that obtained after 1 h, a decrease in the 542 and 577 nm absorption bands is observed, indicative of the oxyhemoglobin consumption. Conversely, the appearance of the 500 and 630 nm absorption bands validates the formation of methemoglobin, confirming the reaction of NO with the hemoglobin.[40] The shift in the band at ca. 415 nm to lower wavelengths is also in accord with the transformation of oxyhemoglobin to methemoglobin.

The possibility of the oxidation of hemoglobin by a factor other than the release of NO was checked by performing a control experiment with ETS-4 without being loaded with NO. In this case, no changes in the spectrum of the solution were observed during 1 h (see Figure S6 in the Supporting Information), showing that no oxidation of the oxyhemoglobin occurs when NO is not previously loaded in the ETS-4. Also, the "basal" oxidation of oxyhemoglobin during the period of the experiment could not be observed. Thus, the evidence in Figure 8 is due to the release of NO from ETS-4. These results show that

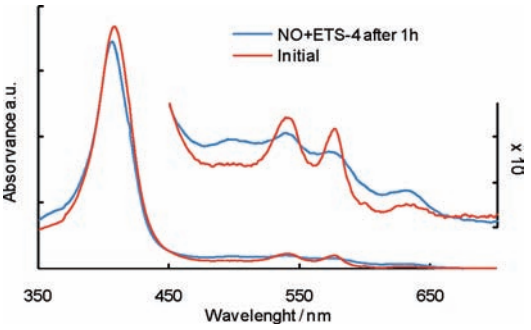

Figure 8. Changes in the UV/vis spectrum of oxyhemoglobin solution upon introduction of ETS-4 loaded with NO. Inset depicts a detail of the spectra between 450 and 700 nm.

ETS-4 is capable of storing and releasing NO with biological activity.

Nevertheless, it is apparent from the observed irreversible adsorption and from the infrared spectra that the adsorption of NO on porous materials for controlled release must take into account the possible formation of other nitrogen oxide species. Besides those identified in the infrared results, the formation of nitrate ions by reaction with lattice oxygen atoms is also possible.[41−43] These reasons could explain why the amount of released NO estimated from the oxyhemoglobin assays (about 0.4 μmol g^{-1}) is somehow lower than could be expected from the amounts adsorbed. Another important question is the shelf life of ETS-4 loaded with NO, which needs to be carefully studied before therapeutic applications. Further work is needed to address these issues.

However, the results already obtained indicate that the release rates may be tuned by the judicious choice of the titanosilicate adsorbent. In particular, ETS-4 presents considerable potential as a slow release NO agent for being explored in therapeutic applications.

The presence of unsaturated transition-metal centers, such as Ti^{4+}, in the framework of stoichiometric microporous silicates

dx.doi.org/10.1021/ja200663e | J. Am. Chem. Soc. 2011, 133, 6396–6402

provides a new approach for designing NO storage and releasing materials, with high stability and expected low toxicity. This idea was illustrated here with ETS-4, a titanosilicate that displays excellent NO adsorption capacity and a slow releasing kinetics. Because layered titanosilicates containing pentacoordinated Ti^{4+} are available,[44,45] this concept may be extended to lower dimensionality solids, perhaps exploring intercalation and pillaring chemistry. Work along these lines is in progress.

■ ASSOCIATED CONTENT

Supporting Information. Nitrogen adsorption isotherms, at −196 °C, on the studied materials; kinetic profiles of NO adsorption and desorption on ETS-10, at 25 °C, after outgassing at 100 and 300 °C; TGDSC results obtained with samples after being exposed to NO; DRIFT spectra of samples after 1 week with 80 kPa NO and then being degassed; views of the optimized configurations of N_xO_y species on the $(TiO_5)Si_4O_{10}H_8$ cluster; UV−vis spectrum of the oxyhemoglobin solution upon introduction of ETS-4 (not loaded with NO); and complete ref 28. This material is available free of charge via the Internet at http://pubs.acs.org.

■ AUTHOR INFORMATION

Corresponding Author
rocha@ua.pt

■ ACKNOWLEDGMENT

We acknowledge FEDER, FSE, and FCT for a postdoctoral grant (BPD/26559/2006), for the project PTDC/CTM/73243/2006, and for the Programa Ciência 2007.

■ REFERENCES

(1) Moncada, S.; Palmer, R. M. J.; Higgs, E. A. *Pharmacol. Rev.* **1991**, *43*, 109–142.
(2) Keefer, L. K. *Nat. Mater.* **2003**, *2*, 357–358.
(3) Morris, R. E.; Wheatley, P. S. *Angew. Chem., Int. Ed.* **2008**, *47*, 4966–4981.
(4) Murphy, E. J.; Roberts, E.; Horrocks, L. A. *Neuroscience* **1993**, *55*, 597–605.
(5) Murphy, E. J.; Roberts, E.; Anderson, D. K.; Horrocks, L. A. *Neuroscience* **1993**, *57*, 483–490.
(6) Petushkov, A.; Intra, J.; Graham, J. B.; Larsen, S. C.; Salem, A. K. *Chem. Res. Toxicol.* **2009**, *22*, 1359–1368.
(7) Hudson, S. P.; Padera, R. F.; Langer, R.; Kohane, D. S. *Biomaterials* **2008**, *29*, 4045–4055.
(8) Mowbray, M.; Tan, X.; Wheatley, P. S.; Morris, R. E.; Weller, R. *J. Invest. Dermatol.* **2006**, *126*, 102–102.
(9) Wheatley, P. S.; Butler, A. R.; Crane, M. S.; Fox, S.; Xiao, B.; Rossi, A. G.; Megson, I. L.; Morris, R. E. *J. Am. Chem. Soc.* **2006**, *128*, 502–509.
(10) Xiao, B.; Wheatley, P. S.; Zhao, X. B.; Fletcher, A. J.; Fox, S.; Rossi, A. G.; Megson, I. L.; Bordiga, S.; Regli, L.; Thomas, K. M.; Morris, R. E. *J. Am. Chem. Soc.* **2007**, *129*, 1203–1209.
(11) McKinlay, A. C.; Xiao, B.; Wragg, D. S.; Wheatley, P. S.; Megson, I. L.; Morris, R. E. *J. Am. Chem. Soc.* **2008**, *130*, 10440–10444.
(12) Nair, S.; Jeong, H. K.; Chandrasekaran, A.; Braunbarth, C. M.; Tsapatsis, M.; Kuznicki, S. M. *Chem. Mater.* **2001**, *13*, 4247–4254.
(13) Anderson, M. W.; Terasaki, O.; Ohsuna, T.; Philippou, A.; Mackay, S. P.; Ferreira, A.; Rocha, J.; Lidin, S. *Nature* **1994**, *367*, 347–351.
(14) Carvalho, M. B.; Pires, J.; Carvalho, A. P. *Microporous Mater.* **1996**, *6*, 65–77.
(15) Pires, J.; Carvalho, M. B.; Carvalho, A. P. *Zeolites* **1997**, *19*, 107–113.
(16) Rocha, J.; Ferreira, A.; Lin, Z.; Anderson, M. W. *Microporous Mesoporous Mater.* **1998**, *23*, 253–263.
(17) Fletcher, A. J.; Kennedy, M. J.; Zhao, X. B.; Bell, J. G.; Thomas, K. M. In *Recent Advances in Adsorption Processes for Environmental Protection and Security*; Mota, J. P., Lyubchik, S., Eds.; Springer: Dordrecht, 2008; pp 29−54.
(18) Kresse, G.; Hafner, J. *Phys. Rev. B* **1993**, *47*, 558–561.
(19) Kresse, G.; Furthmüller, J. *Comput. Mater. Sci.* **1996**, *6*, 15–50.
(20) Kresse, G.; Furthmüller, J. *Phys. Rev. B* **1996**, *54*, 11169–11186.
(21) Perdew, J. P.; Burke, K.; Ernzerhof, M. *Phys. Rev. Lett.* **1996**, *77*, 3865–3868.
(22) Blöchl, P. E. *Phys. Rev.* **1994**, *50*, 17953.
(23) Kresse, G.; Joubert, D. *Phys. Rev. B* **1999**, *59*, 1758–1775.
(24) Gomes, J. R. B.; Cordeiro, M. N. D. S.; Jorge, M. *Geochim. Cosmochim. Acta* **2008**, *72*, 4421–4439.
(25) Becke, A. D. *Phys. Rev. A* **1988**, *38*, 3098–3100.
(26) Lee, C. T.; Yang, W. T.; Parr, R. G. *Phys. Rev. B* **1988**, *37*, 785–789.
(27) Becke, A. D. *J. Chem. Phys.* **1993**, *98*, 5648–5652.
(28) Frisch, M. J.; et al. *Gaussian 03*, revision D.02; Gaussian, Inc.: Wallingford, CT, 2004.
(29) Krishnan, R.; Binkley, J. S.; Seeger, R.; Pople, J. A. *J. Chem. Phys.* **1980**, *72*, 650–654.
(30) Blaudeau, J. P.; McGrath, M. P.; Curtiss, L. A.; Radom, L. *J. Chem. Phys.* **1997**, *107*, 5016–5021.
(31) Hay, P. J.; Wadt, W. R. *J. Chem. Phys.* **1985**, *82*, 270–283.
(32) Merrick, J. P.; Moran, D.; Radom, L. *J. Phys. Chem. A* **2007**, *111*, 11683–11700.
(33) Valero, R.; Gomes, J. R. B.; Truhlar, D. G.; Illas, F. *J. Chem. Phys.* **2010**, *132*, 104701–104713.
(34) Paul, D. K.; Smith, B. W.; Marten, C. D.; Burchett, J. *J. Mol. Catal. A* **2001**, *167*, 67–79.
(35) Matsumoto, A.; Sano, M.; Nishimiya, N.; Tsutsumi, K. *Adsorption* **2000**, *6*, 251–257.
(36) Chao, C. C.; Lunsford, J. H. *J. Am. Chem. Soc.* **1971**, *93*, 6794–6800.
(37) Katoh, M.; Yamazaki, T.; Kamijo, H.; Ozawa, S. *Zeolites* **1995**, *15*, 591–596.
(38) Zhang, W. X.; Yahiro, H.; Iwamoto, M.; Izumi, J. *J. Chem. Soc., Faraday Trans.* **1995**, *91*, 767–771.
(39) Zecchina, A.; Arean, C. O.; Palomino, G. T.; Geobaldo, F.; Lamberti, C.; Spoto, G.; Bordiga, S. *Phys. Chem. Chem. Phys.* **1999**, *1*, 1649–1657.
(40) Feelisch, M.; Kubitzek, D.; Werringloer, J. In *Methods in Nitric Oxide Research*; Feelisch, M., Stamler, J. S., Eds.; John Wiley & Sons, Ltd.: New York, 1996; pp 455−478.
(41) Li, G. H.; Jones, C. A.; Grassian, V. H.; Larsen, S. C. *J. Catal.* **2005**, *234*, 401–413.
(42) Yeom, Y. H.; Henao, J.; Li, M. J.; Sachtler, W. M. H.; Weitz, E. *J. Catal.* **2005**, *231*, 181–193.
(43) Sedlmair, C.; Gil, B.; Seshan, K.; Jentys, A.; Lercher, J. A. *Phys. Chem. Chem. Phys.* **2003**, *5*, 1897–1905.
(44) Roberts, M. A.; Sankar, G.; Thomas, J. M.; Jones, R. H.; Du, H.; Chen, J.; Pang, W.; Xu, R. *Nature* **1996**, *381*, 401–404.
(45) Lin, Z.; Rocha, J.; Brandao, P.; Ferreira, A.; Esculcas, A. P.; Jesus, J. D. P.; Philippou, A.; Anderson, M. W. *J. Phys. Chem. B* **1997**, *101*, 7114–7120.
(46) Rouquérol, F.; Rouquerol, J.; Sing, K. *Adsorption by Powders and Porous Solids*; Academic Press: San Diego, CA, 1999.
(47) Rusu, C. N.; Yates, J. T. *J. Phys. Chem. B* **2001**, *105*, 2596–2603.